Supporting Information

Structural features, dissolution performance and anthelmintic efficacy of multicomponent solid forms of fenbendazole with maleic and oxalic acids

Artem O. Surov[a], Nikita A. Vasilev[a], Oxana V. Magdysyuk[b], German L. Perlovich[a,] Anastasiya I. Varlamova[c], Ivan A. Arkhipov[c], Irina M. Odoevskaya[c]*

[a]G.A. Krestov Institute of Solution Chemistry RAS, 153045, Ivanovo, Russia.

[b]Diamond Light Source Ltd, Harwell Science and Innovation Campus, Didcot, OX11 0DE, UK

[c]Federal State Budget Scientific Institution "Federal Scientific Centre VIEV", B. Cheremushkinskaya street 28, 117218 Moscow, Russia

*To whom correspondence should be addressed: Telephone: +7-4932-533784; Fax: +7-4932-336237; E-mail glp@isc-ras.ru

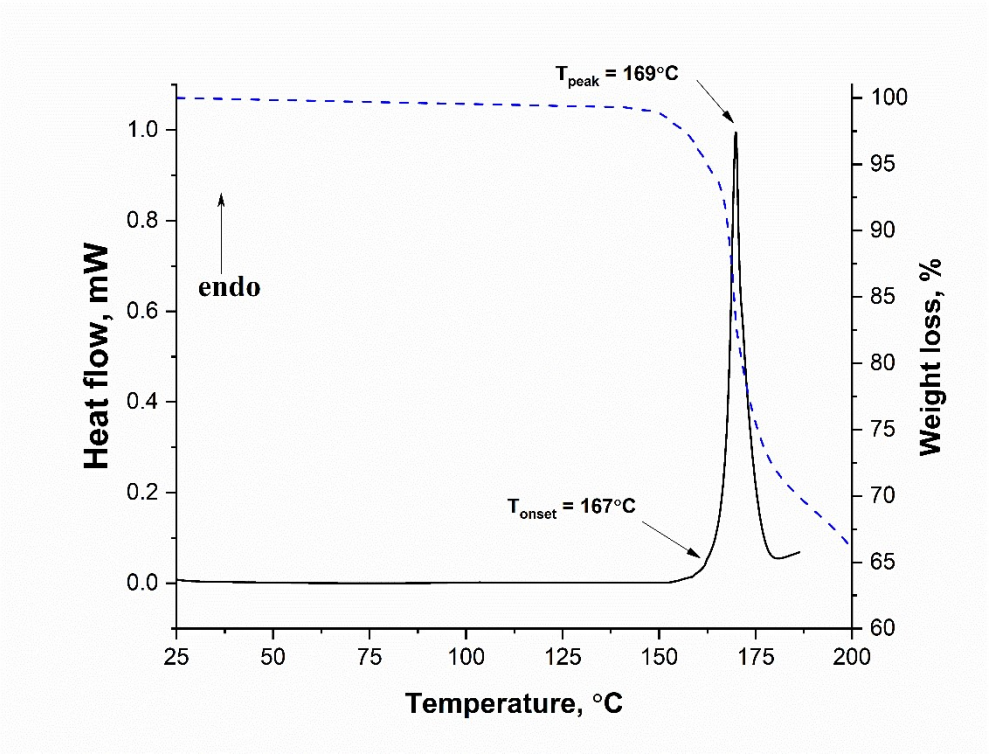

Figure S1. Results of DSC and TGA analyses of **[FNB+Mal] (1:1)**

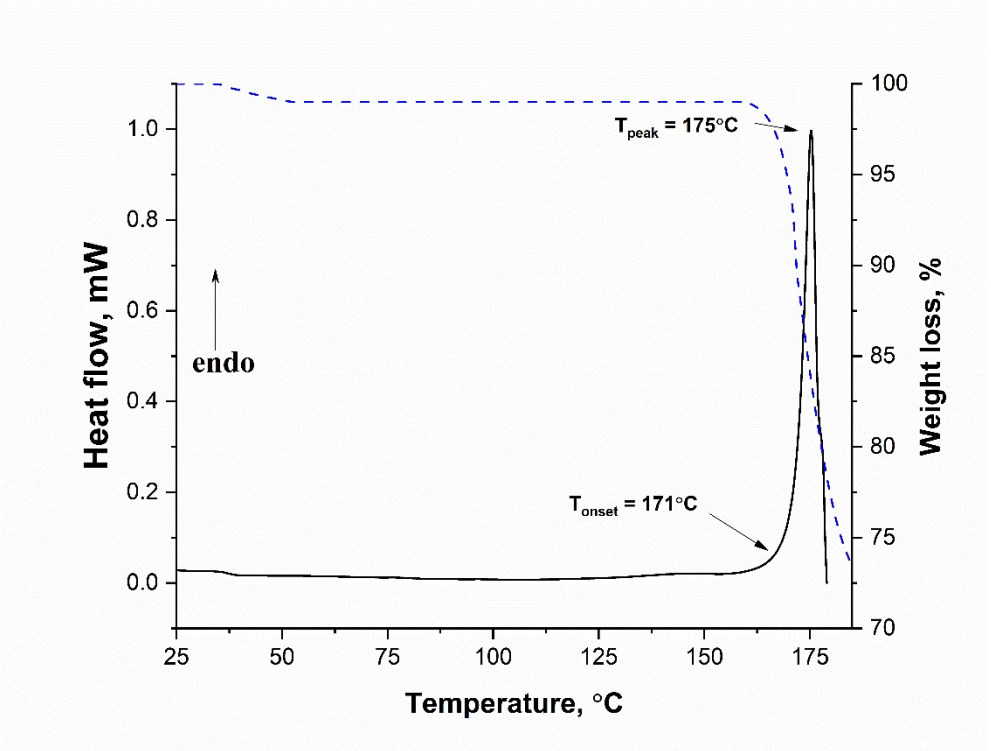

Figure S2. Results of DSC and TGA analyses of **[FNB+Ox] (1:1)**

(a) (b)

Figure S3. Illustration of starting structural models of a salt (a) and a cocrystal (b) used for the subsequent periodic DFT-D geometry optimization.

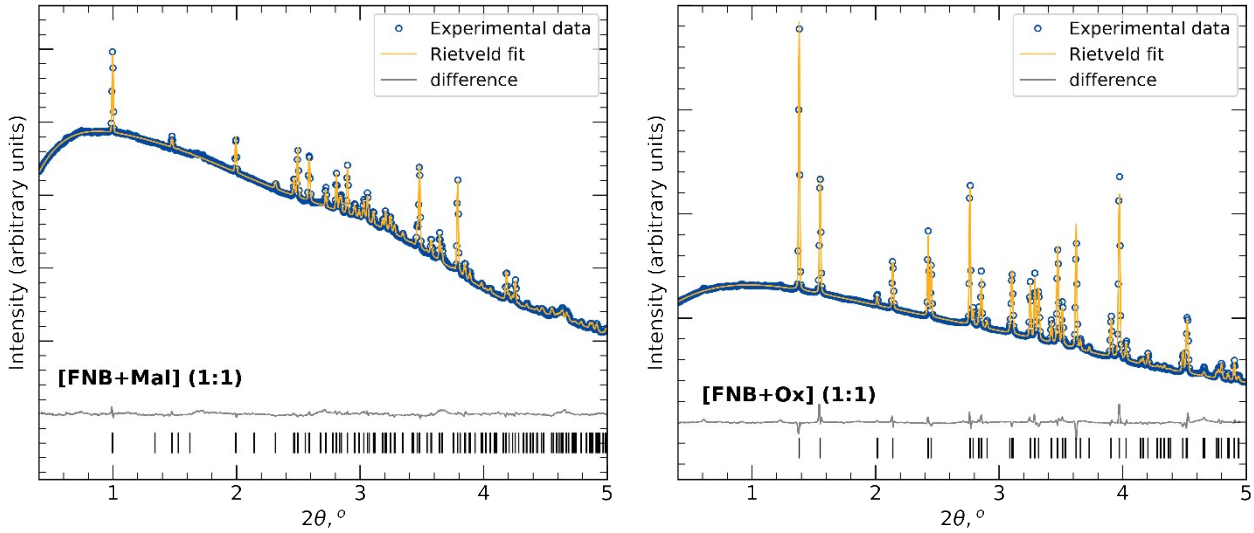

(a) (b)

Figure S4. Powder diffraction refinement for (a) **[FNB+Mal]** (1:1), (b) [**FNB+Ox**] (1:1).

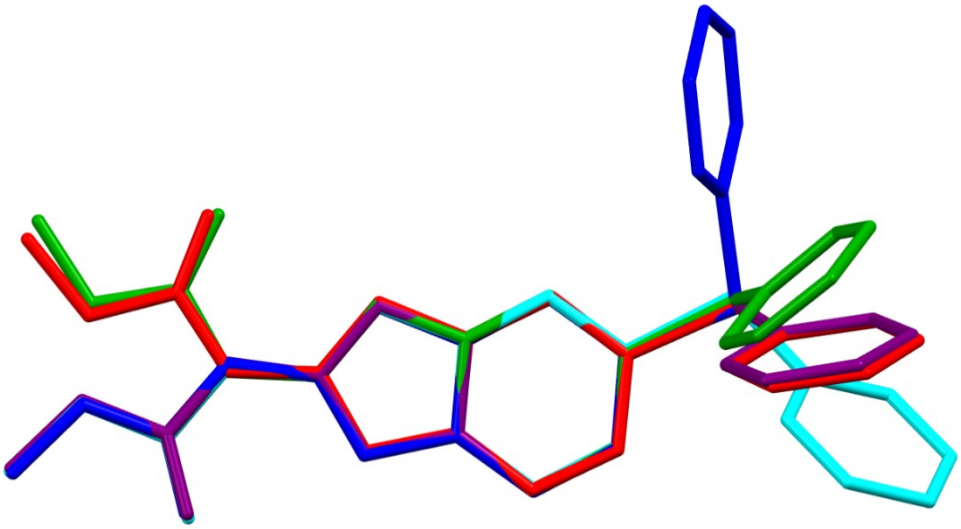

Figure S5. Overlay of the FNB conformations in the crystals of [**FNB+Mal**] (1:1) (red), **[FNB+Ox] (1:1)** (blue), [**FNB+MSA**] (1:1) (cyan), [**FNB+TSA+H_2O**] (1:1:1) (purple) and [**FNB+TSA**] (1:1) (green)

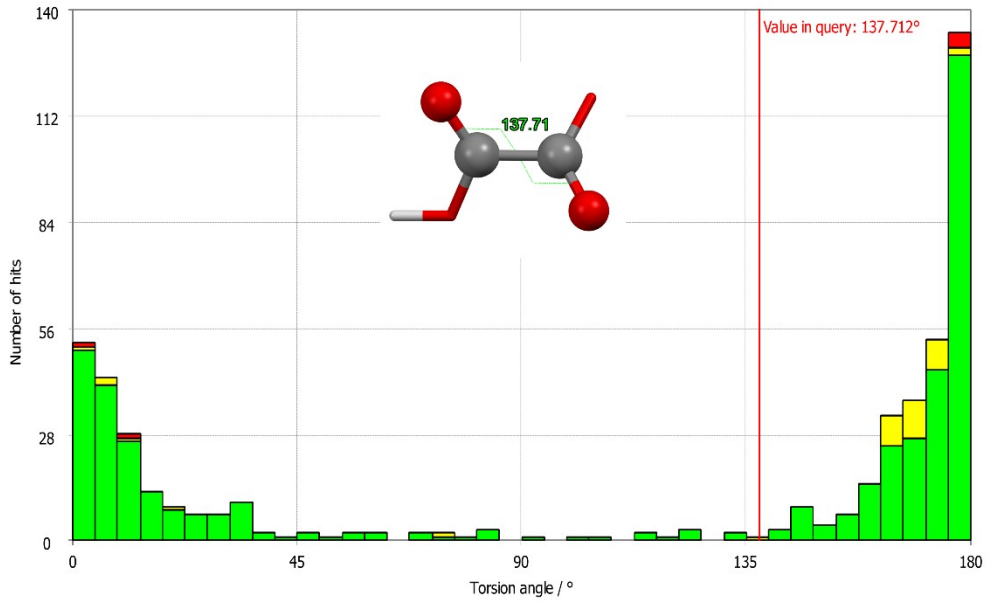

Figure S6. Results of the Mogul analysis for the torsion angle responsible for orientation of the deprotonated and protonated carboxyl groups in the oxalate ion. The target torsion angle is highlighted in the inserted figure

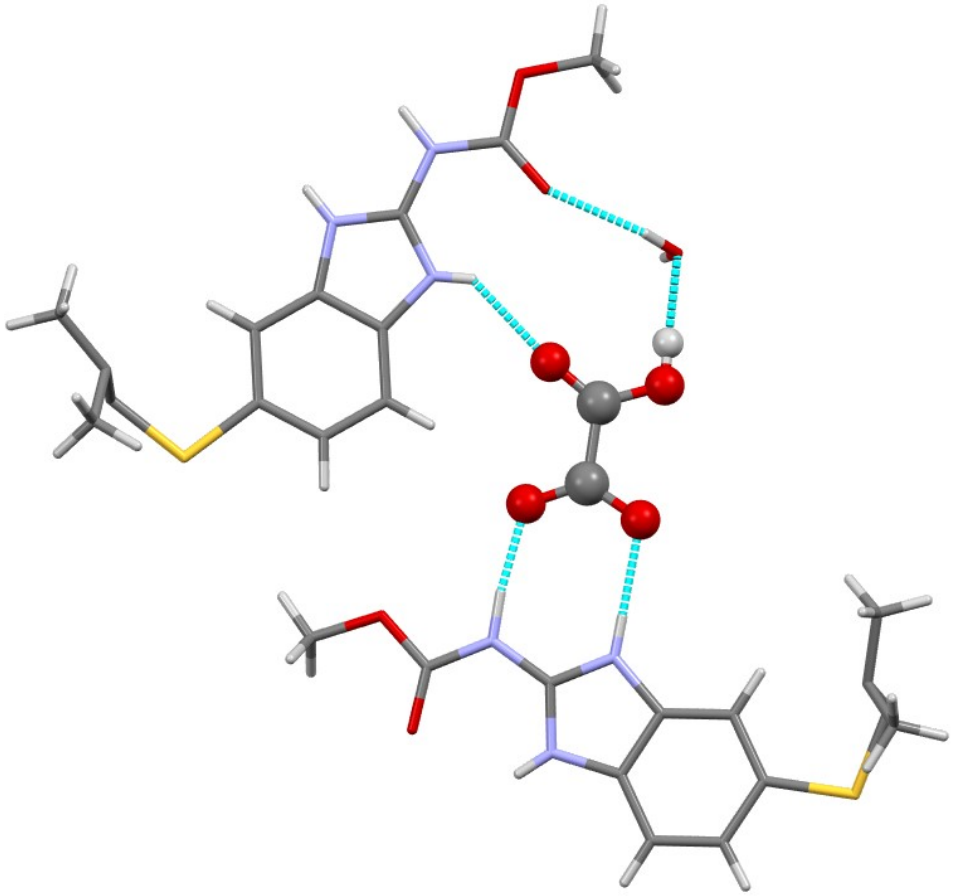

Figure S7. Illustration of hydrogen bonding motifs in the crystal structure of monohydrate of albendazole oxalate

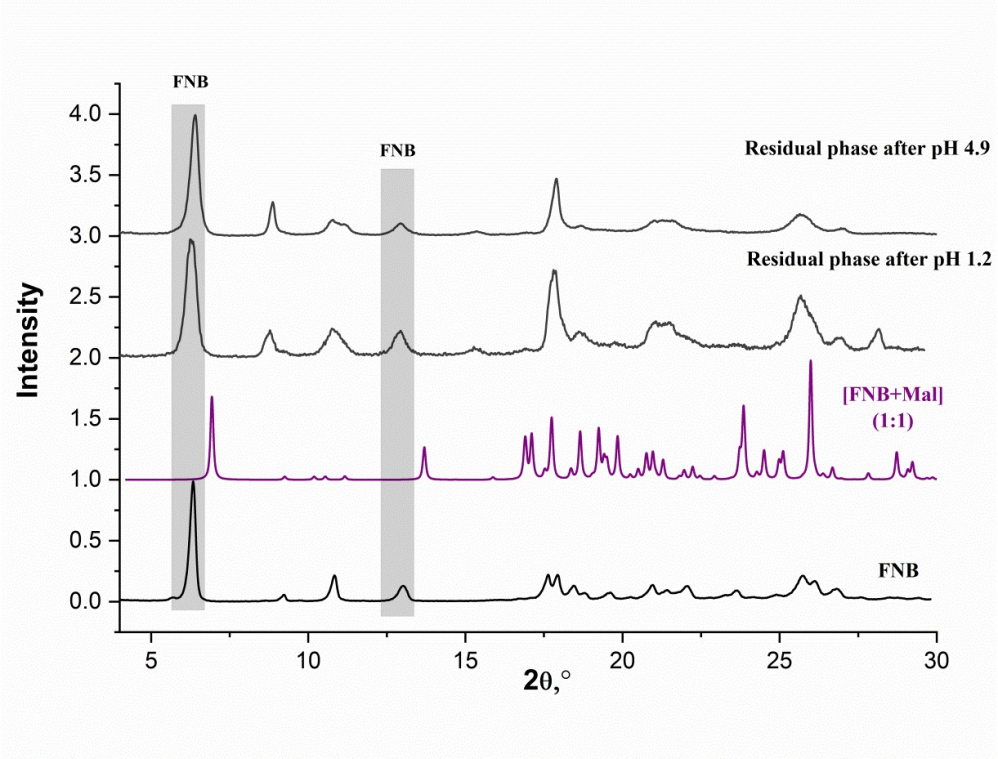

Figure S8. Experimental PXRD patterns of residual materials after dissolution experiments for **[FNB+Mal]** (1:1) at pH 1.2 and pH 4.9

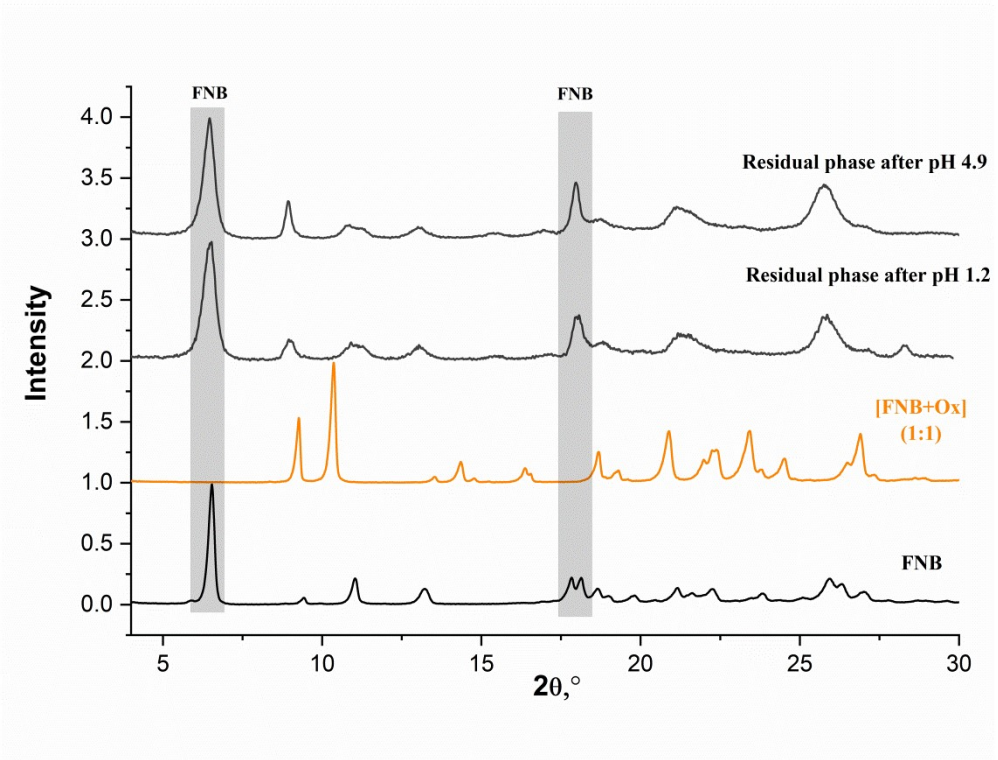

Figure S9. Experimental PXRD patterns of residual materials after dissolution experiments for **[FNB+Ox]** (1:1) at pH 1.2 and pH 4.9

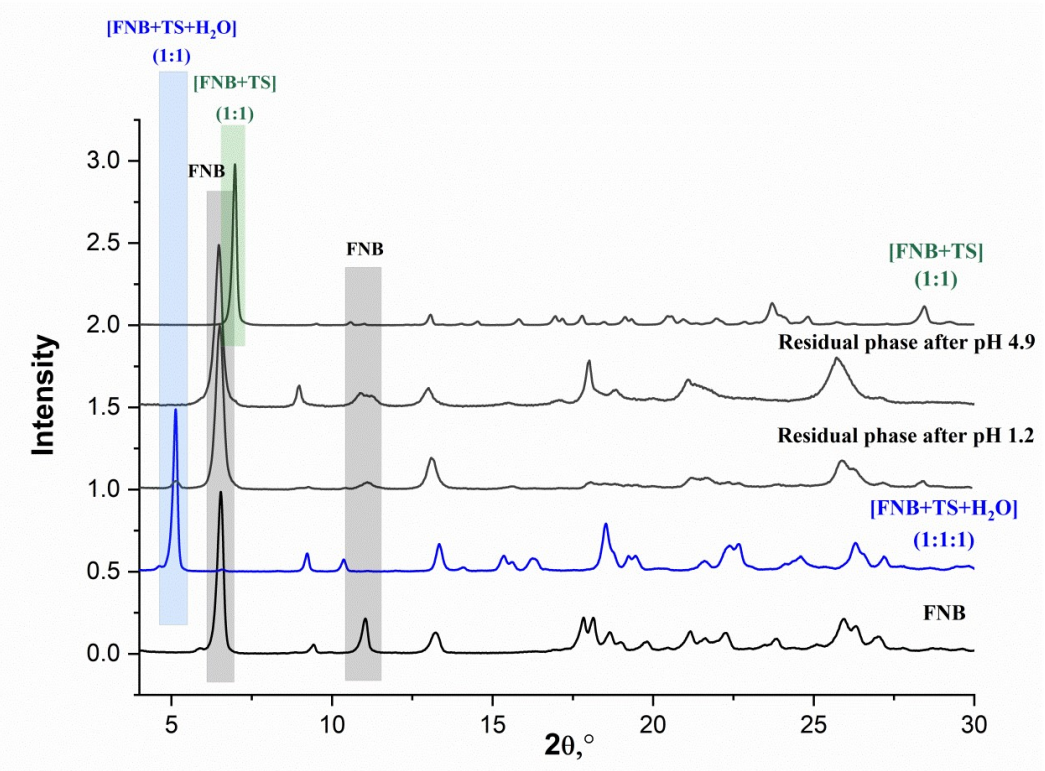

Figure S10. Experimental PXRD patterns of residual materials after dissolution experiments for **[FNB+TS]** (1:1) at pH 1.2 and pH 4.9

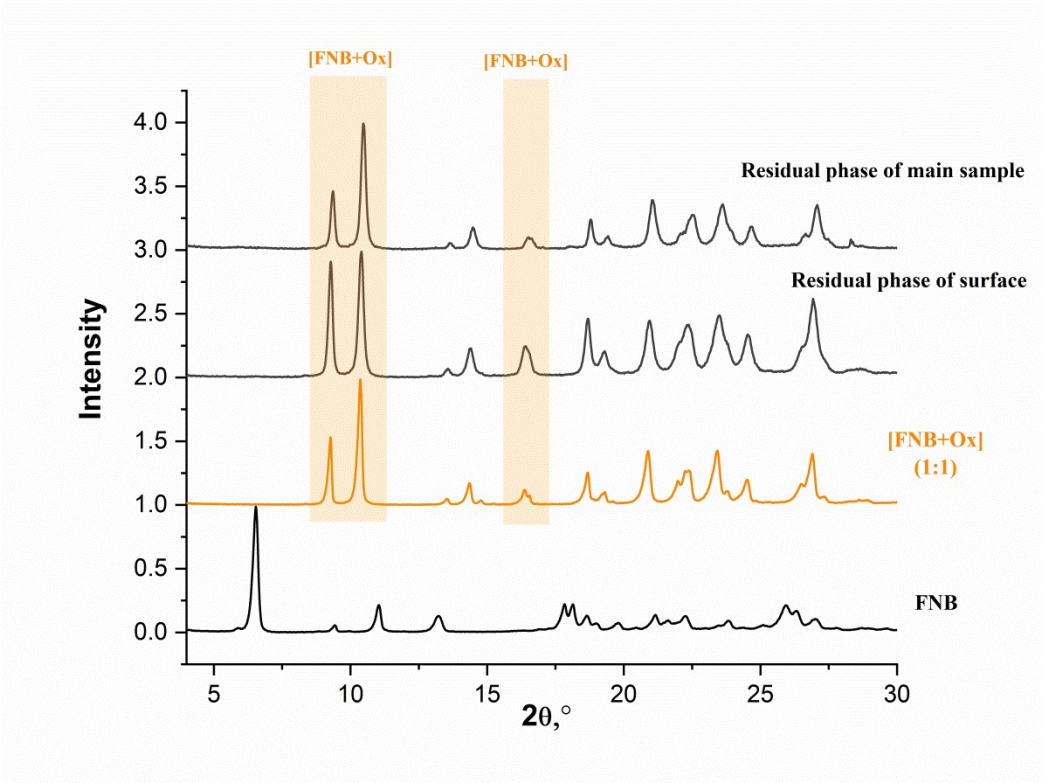

Figure S11. Experimental PXRD patterns of residual materials after IDR experiments for **[FNB+Ox]** (1:1) at pH 1.2

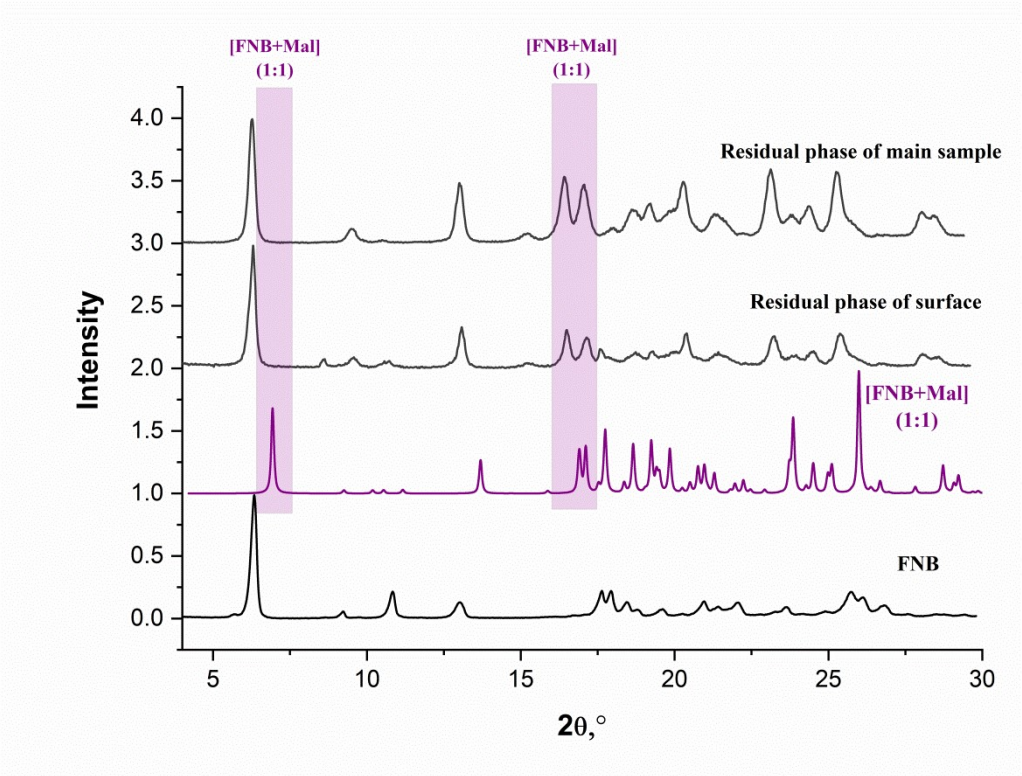

Figure S12. Experimental PXRD patterns of residual materials after IDR experiments for **[FNB+Mal]** (1:1) at pH 1.2

Table S1. Crystallographic data for FNB salts

Compound reference	[**FNB+Mal**] (1:1)	[**FNB+Ox**] (1:1)
CCDC number	2221519	2221520
Chemical formula	$C_{15}H_{13}N_3O_2S \cdot C_4H_4O_4$	$C_{15}H_{13}N_3O_2S \cdot C_2H_2O_4$
*F*w	415.42	389.38
Crystal system	Monoclinic	Monoclinic
a, Å	17.7039(11)	26.15106(90)
b, Å	19.5216(12)	5.62505(16)
c, Å	5.51938(27)	16.88572(40)
α, °	90	90
β, °	91.1706(27)	46.3627(19)
γ, °	90	90
Unit cell volume, Å^3	1907.2(2)	1797.66(11)
Temperature, K	293	293
Space group	$P2_1/n$	Cc
No. of formula units per unit cell, *Z*	4	4
Radiation wavelength, Å	0.22826	0.22826
Absorption coefficient, $\mu \cdot mm^{-1}$	0.032	0.032
R_{wp}	0.0065	0.0172
R_B	0.0351	0.0572

Table S2. Dissolution parameters in 1.2 and 4.9 Buffer Media at 37°C.

$pH_{initial}$	Solid forms	AUC_{0-360}, mg·min/ml
1.2	FNB	4.34 ± 0.40
	[FNB+Mal] (1:1)	13.39 ± 0.33
	[FNB+Ox] (1:1)	15.78 ± 0.45
	[FNB+TS] (1:1)	30.67 ± 0.50
4.9	FNB	0.14 ± 0.03
	[FNB+Mal] (1:1)	0.20 ± 0.04
	[FNB+Ox] (1:1)	0.17 ± 0.04
	[FNB+TS] (1:1)	0.28 ± 0.02

Table S3. Efficacy of FNB and its salts against *Trichinella spiralis* infection in mice

Dose of 140 larvae per animal			
Substance	Dose, mg/kg of API	Number of mice in group	Efficacy (%)[a]
FNB	2	10	43.6 ± 4.3
[FNB+Ox]	2	10	37.1 ± 5.5
[FNB+Mal]	2	10	39.0 ± 4.9
[FNB+TS]	2	10	83.5 ± 5.9
Dose of 200 larvae per animal			
FNB	2	10	55.1 ± 4.0
[FNB+TS]	2	10	88.2 ± 5.5

[a]- calculated based on the number of discovered helminths in the experiment and control